SSC24-WI-07

Performance Analysis of a Pointing, Acquisition, and Tracking System for the VISION Laser Crosslink Mission

Yeji Kim, Pureum Kim, Han-Gyeol Ryu, Sang-Young Park
Astrodynamics and Control Laboratory, Yonsei University
Science Hall, 50 Yonsei-ro, Seodaemun-gu, Seoul, Republic of Korea
dpwl4353@yonsei.ac.kr

ABSTRACT

As the volume of space-borne data increases, laser communication techniques are being considered to achieve a fast transmission rate and high link security or privacy. The very-high-speed intersatellite link system using an infrared optical terminal and nanosatellite (VISION) mission comprises two 6U formation-flying nanosatellites, and its main objective is to achieve a Gbps-level inter-satellite data-transfer capacity by applying laser communication technology in free space. A pointing, acquisition, and tracking (PAT) system is required to establish and maintain a stable laser crosslink. In the CubeSat platform, the PAT system relies on a satellite attitude determination and control system (ADCS) for body pointing, owing to its low size, weight, and power (SWaP) constraints. Precise orbit/attitude determination and control techniques primarily determine the availability of a coarse pointing system before entering a fast-steering mirror (FSM) feedback loop system with a laser communication terminal (LCT). This study focused on developing a software orbit-attitude integrated simulator to analyze the performance of the PAT system in the VISION mission scenario. An orbit-attitude integrated simulator was designed to test and validate the PAT sequence of the bus initialization stage (BIS) and coarse PAT stage (CPS) with short-wave infrared camera (CAM) feedback. By applying the characteristics of the CubeSat, absolute and relative navigation systems, star trackers, and control hardware, numerical assessments were conducted to evaluate the body pointing performance during the PAT sequence caused by internal or external disturbances in the VISION mission scenario. The simulation results give a total body pointing error of 46.94 arcsec (3σ), indicating that the attitude control system combined with the developed navigation model satisfies the total body pointing error budget within 90 arcsec (3σ) in the PAT system.

INTRODUCTION

A non-terrestrial network (NTN) consists of various space-borne and aerial communication networks, including geosynchronous equatorial orbit (GEO), medium Earth orbit (MEO), and low Earth orbit (LEO) satellite constellations, achieving universal coverage and on-demand capacity.[1] The NTN can provide extensive coverage in aircraft, ocean, and rural areas with a high-speed data transmission rate to supplement traditional terrestrial network (TN) communications. The 3rd Generation Partnership project (3GPP) has categorized NTN communication via GEO, LEO satellites, and flying unmanned aircraft systems (UAS).[2] In GEO and UAS platforms, where long propagation delays and limited coverage problems are considered the primary drawbacks in achieving a free-space optical communication (FSOC) system. However, LEO satellites are more suitable for FSOC because of their high orbital velocity and low altitude. The FSOC in LEO environments enables fast data transmission at rates greater than 1 Gbps with high link security, which is difficult to achieve using traditional radio frequency (RF) systems. To deal with the growing volume of spaceborne data involving defense applications, progress has been made in the development of commercial satellite constellations in LEO, such as Starlink, OneWeb, TeleSat, and Amazon.

Although most communication satellites have been developed using large satellite bus systems, the recent demand for leveraging cube/nanosatellites in space applications is rapidly growing because of their efficient size, weight, and power (SWaP) properties. CubeSats have an advantage in that they have low launch, experiment, and design-and-deployment costs, as well as their applicability for a variety of space missions.[3, 4, 5] However, the low on-board processing capability and their limited structural design are the main challenges in CubeSat platforms, leading to a limited mission life and range of travel.[6, 7] Particularly when substantial

quantities of data are required in CubeSat operations, the data demand can be well beyond the capacity of traditional radio frequency (RF) communication systems owing to the constraints imposed by SWaP limitations.[8]

Despite these challenges, Kaushal et al[9] and Carrasco-Casado et al[10] successfully analyzed the feasibility of FSOC using an intersatellite link. Future space technologies are now focusing on the prospects of the CubeSat platform to develop a laser communication (lasercom) or FSOC link system.[11] The applicability of lasercom techniques in CubeSat platforms has successfully been demonstrated in past and ongoing missions; by demonstrating an optical downlink using AeroCube-OCSD,[12] by developing a proprietary and patented miniature low-power, high-performance laser communication terminal of LaserCube,[13] and by building the world's smallest Laser Communication Terminal from satellite to ground links using CubeLCT.[14] As space lasercom missions continue to be attempted through formation flight or swarm operation techniques of CubeSats, the PIXL-1 and Cubesat Laser Infrared CrosslinK (CLICK) have even advanced the lasercom objectives. Because of the SWaP and cost limitations of CubeSat platforms, pointing, acquisition, and tracking (PAT) systems rely on a satellite's attitude determination and control system (ADCS) to achieve precise body pointing.[15]

The main objective of the PIXL-1 mission is to demonstrate higher data rates from satellites to ground stations and to enable further projects within the framework of optical satellite communications using two 3U CubeSats.[16] It contain an optical demonstration payload, CubeLCT, and its terminal supports up to 100 Mbps in the downlink over a relative distance of up to 1,500 km, achieving an output power of 1 W.[17] The CubeSat was developed by the German Aerospace Center (DLR) and was successfully launched in January 2021. Its attitude control system requires a very fine accuracy of ±0.1 deg to achieve laser lock in a reasonable time.[14]

The CLICK-B/C is planned to launch in 2024 to achieve a 20 Mbps intersatellite optical crosslink and precision ranging between two 3U CubeSats, which has been jointly developed by MIT and NASA ARC.[18] Maintaining a relative distance from 25 km to 580 km, a payload power draw of 3.95 W and a tracking error of below 1 μrad are achieved. Because one of the major challenges in the CubeSat Lasercom is the development of a PAT system to establish and maintain laser links, the CLICK coarse pointing system directly utilizes the spacecraft's ADCS.[19]

The very-high-speed intersatellite link system that uses an infrared optical terminal and nanosatellite (VISION) mission comprises two 6U formation-flying nanosatellites. The mission aims to establish the FSOC in free space with a data-transmission rate of 1 Gbps and maintain the laser crosslink for over 10 min.[20] For achieving a stable crosslink and high-speed data transfer, the precise pointing and tracking of the laser links are assisted by the attitude control system and the real-time relative navigation technique. The PAT system of VISION holds the pointing error budgets of the point-ahead and tracking errors, and the point-ahead error consists mainly of attitude control and relative navigation errors. To successfully generate attitude commands for the ADCS module to align the payload aboard the CubeSat body, we utilized a real-time relative navigation algorithm to estimate the positioning and pointing accuracies of the spacecraft body and its payload.

In this study, a software orbit-attitude integrated simulator was developed to analyze the performance of the PAT system in the VISION mission scenario. An attitude control system with three-axis reaction wheels (RWs) was utilized to assist in the alignment of the two satellites with respect to line-of-sight (LOS) vectors. By applying the characteristics of CubeSats, absolute and relative navigation systems, star trackers, and control hardware, we conducted numerical assessments of the positioning and pointing errors during the PAT sequence caused by internal or external disturbances in the VISION mission scenario. The body-pointing error for the PAT sequence is discussed to demonstrate that the attitude control system combined with the developed navigation model satisfies the mission requirements of the PAT system.

This paper provides an overview of the VISION mission and its requirements for PAT systems. The detailed system of pointing, acquisition, and tracking during the mission is then addressed. The implementation of the integrated orbit-attitude simulator and its results are described. Finally, the conclusions of the study are presented.

The VISION mission

The main objective of the VISION mission is to achieve a Gbps-level inter-satellite data-transfer capacity by applying laser communication technology in free space, which comprises two 6U formation-flying nanosatellites.[20] The two spacecraft will be operated in LEO and long baseline environments, maintaining the goal of establishing and validating laser-crosslink systems at intersatellite distances of up to 1,000 km. Two formation-flying nanosatellites (Altair and Vega) were aligned along the track direction, achieving a super-high

data transmission rate of 1 Gbps, which was maintained for over 10 min (Figure 1).

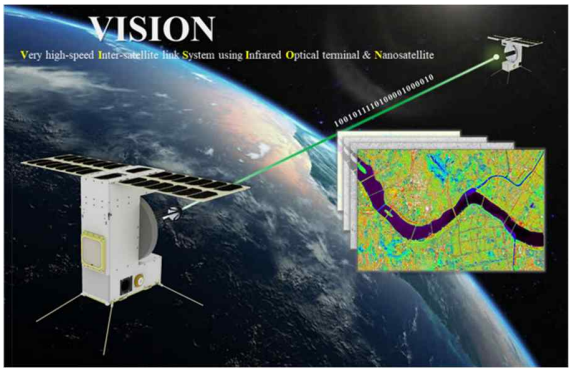

Figure 1: Concept of the VISION mission[20]

The mission lifetime is longer than one year, and the systems are developed aboard a standard 6U nanosatellite.[21] Its payload system is based on a laser communication terminal (LCT) containing deployable front-end optics to gain optical power to enable beam transmission and reception. For establishing a stable crosslink, the optical axes of each nanosatellite are aligned and reduce the residual error sources such as jitter smaller than 1 μrad to ensure the optical link performance with respect to the LOS vector.[20] The PAT sequence is required to precisely align the LOS vectors between formation-flying satellites. In an optical laser crosslink, the transmission beam should be narrower than that of a typical radio frequency carrier. Therefore, multiple sequences for mitigating look-angle errors in a step-by-step manner are required with the developed payload, orbit/attitude determination, and control systems. In a closed-loop system, the payload can reduce the steady-state error and remaining jitter by utilizing a fast-steering mirror (FSM).

To execute the PAT system, an integrated ADCS (XACT-50, Blue Canyon Technologies) with three-axis RWs was installed in the CubeSat bus, whereas real-time relative navigation formulated a target LOS vector to support command generation for the integrated ADCS. The relative navigation technique relies on an S-band intersatellite crosslink (ISL) to exchange GPS raw data of the L1/L2 signals. Dual-frequency bands are essential for addressing ionospheric delay errors in long baseline scenarios. They can be modeled using estimation algorithms such as the Kalman filter without the implementation of the ionospheric-free combinations suggested by Odijk[22]. An onboard global navigation satellite system (GNSS) receiver (OEM719, NovAtel) was used to receive and process the GPS observations at a frequency of 1 Hz. The precise formation-flying technique was assisted by an integrated ADCS for the pointing maneuvers.

The VISION mission is classified into three orbital phases, as shown in Figure 2: (1) launch and early orbit phase (LEOP), (2) drift recovery and station keeping phase (DRSKP), and (3) normal operation phase (NOP).[20] The initially stabilizes the CubeSat bodies after separation from the launch vehicle and deploys the antenna and solar panel for power charging and UHF communication with the ground station. In the DRSKP, Altair and Vega are separated by relative distances of up to 1,000 km, and the separation is narrowed to 50 km again with the thrusters in the desired direction. The crosslinks between the two CubeSats were tested by station-keeping to check the availability of S-band communications. The NOP finally activated the actual formation-flying techniques for baselines, including 50, 100, 200, 500, and 1,000 km to evaluate the performance of the crosslink. Real-time relative navigation was utilized to assist precise pointing with the dual-frequency GPS signals, and the integrated ADCS module was mainly used to align the LOS vectors of each satellite with three-axis RWs.

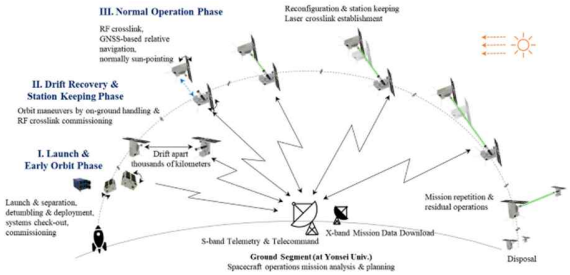

Figure 2: Operations of the VISION mission[20]

When navigation and attitude control systems successfully reduce the pointing uncertainties to locate the beam within the full field of view of a short-wave infrared camera (CAM), the deployable payload can also be used to compensate for the pointing bias and satisfy the pointing requirements in terms of the angle of arrival (AOA). The residual jitter was then mitigated using the FSM to enhance the performance of the laser crosslink.

The sequential process of establishing and maintaining the laser crosslink is called the PAT sequence, classified into three stages: (1) bus initialization stage (BIS), (2) coarse PAT stage (CPS), and (3) fine PAT stage (FPS).[21] During the BIS, the target LOS vectors of two formation-flying satellites are generated by real-time relative navigation based on the carrier-phase-based differential GPS (CDGPS) technique using the GPS raw data of L1/L2 signals exchanged from an S-band intersatellite crosslink (ISL) to achieve a sub-meter relative position uncertainty.[23] The attitude control system with three-axis RWs is also utilized to assist the alignment of the two satellites with respect to the LOS vectors. In a CPS, a broad beam is transmitted to the CAM, potentially resulting in a bias called the angle of arrival (AOA). The

CAM feedback was then executed to correct the AOA. Finally, the FPS reduced the residual jitter to improve the precision of the beam with respect to the LOS vector. Proper operation of the bus and payload enables laser crosslinking for the FSOC by activating the PAT sequence and achieving fast data transmission at rates greater than 1 Gbps with high link security.

Mission requirements

The detailed pointing error requirement for establishing a laser crosslink system is described in Table 1, where μ indicates the bias and σ is the standard deviation error. Using three-axis RWs, two formation-flying CubeSat bodies were aligned with the optical axes of each satellite. The error requirement includes attitude control, alignment, and relative navigation errors, and presents a total pointing error budget for each PAT stage.

In the BIS, the relative navigation (RN) mainly conducts an initial alignment of the formation-flying CubeSat bus and its payload with respect to the LOS vector. The positioning uncertainty must be maintained at less than 60 arcsec at 1,000 km of the baseline and 30 arcsec at 50 km of the baseline, which are converted to 30 m and 3 m, respectively. The BIS requires the bias to be less than 400 μrad and the standard deviation to be less than 60 μrad.

The CPS is divided into three phases: search, acquisition, and detection. Once the CPS search successfully obtains the laser beam in the CAM, CPS acquisition removes control errors or misalignments by calibrating the AOA, followed by CPS detection, which overcomes the remaining LOS jitter by the FSM. The bias of less than 400 μrad and the standard deviation of less than 60 μrad must be maintained in the CPS. For both BIS and CPS, and the mission also requires a pointing error budget of the attitude control system with a total error within 90 arcsec to maintain a stable crosslink and high-speed data transfer (3σ).

The FPS is finally operated with a Quadrant Cell (QC), which is used for the FSM feedback system, whereas the CAM prevents each body from missing the intersatellite beam. It has two sub-stages: hands-off, tracking, and communication. The jitter can be reduced to less than 1 μrad by maintaining precise body pointing error budget of the bias to be less than 30 μrad and the standard deviation to be less than 1 μrad in the FPS. The FPS was not included when investigating pointing performance in this study.

Table 1: Mission requirements on the PAT sequence for the laser crosslink system

Stage	BIS	CPS			FPS	
Duration	~600s	~60s	~180s	~60s	~60s	>600s
Sensor	RN	CAM	CAM AOA	CAM FSM	CAM (QC) FSM	
Total pointing error budget [μrad]	μ < 400 σ < 60	μ < 400 σ < 60			μ < 30 σ < 1	

In the mission, the pointing loss is also required to be less than -14.77 dB for each axis. The transmitted gain loss is also examined and turned out to satisfy the requirements for y and z directions (or pitch and yaw directions) in earth-centered inertial (ECI) frame, considering the ADCS attenuation effect of -5 dB. Even though the gain loss in x axis is -6.5 dB, it does not violate the pointing requirements in x or roll direction. The total perturbation torque was maintained at less than $10^{-6}Nm$, which could be controlled using an XACT-50.

SIMULATION SETUP

An orbital-attitude integrated simulator was designed to test and validate the PAT sequence of the BIS and CPS before entering the FSM feedback system or FPS. By applying the characteristics of the CubeSat, absolute and relative navigation systems, star trackers, and control hardware, we conducted a software simulation of positioning and pointing errors during the PAT sequence caused by internal or external disturbances in the VISION mission scenario. For the PAT system design, we implemented a simulator for each stage to be maintained within the maximum duration, as shown in Table 1. To construct realistic test scenarios, we also considered biased error sources, such as control delay, accumulated angular velocity error, uncertainty of the orbital control systems, misaligned system of the optical payloads, and their thermal deformation. It is known that the major bias error comes from thermal deformation effects, which can be assumed as a fixed value of 100 arcsec, according to Kim[24] in the beam detection process during the BIS.

Dynamic models

To achieve laser crosslinking on CubeSat platforms, ADCS and related navigation techniques are primarily used to initialize and execute the PAT system. The BIS and CPS stages mainly search for the beam and acquire laser crosslinking. For the VISION mission, we implemented an integrated ADCS module (XACT-50) from Blue Canyon Technology. Three-axis RWs control pointing maneuvers. In terms of attitude control disturbances, the sources of error include uncertainty in

the inertial properties, reaction wheel misalignment, sensor noise, sensor misalignment, gyro drift, and onboard timing error.[25] We also implemented orbital perturbations that involve the gravity gradient, air drag, solar radiation, magnetic dipole moment torques, and thrust acceleration of the orbit maneuvers, as expressed in Equation (1).

$$\ddot{\vec{r}} = -\frac{\mu_{\oplus}}{r^3}\vec{r} + \vec{a}_{J2} + \vec{a}_{air} + \vec{a}_{m\,ag} + \vec{a}_{solar} + \vec{a}_{thrust}, \quad (1)$$

where $\vec{r}$ and $\ddot{\vec{r}}$ are the position and acceleration vectors of the satellites, respectively; $\mu_{\oplus}$ indicates the gravitational constant of the Earth; $\vec{a}_{J2}$ is the Earth's gravity gradient torque with J2 perturbation only; $\vec{a}_{air}$ is the air drag acceleration; $\vec{a}_{m\,ag}$ is the magnetic dipole moment torques; $\vec{a}_{solar}$ is the solar radiation pressure acceleration; $\vec{a}_{thrust}$ is the thrust acceleration of the orbit maneuvers of Vega, respectively, with respect to Altair.

Sensor models

The integrated ADCS module consists of four sensors for attitude determination: coarse sun sensor (CSS), magnetometer (MAG), gyro sensor (IMU), and star tracker (STT). The XACT-50 module determines the real-time availability among the sensors according to the Earth, sun, and spacecraft position and attitude information, where the STT is mainly used during the normal operation phase and the PAT sequence. The specifications of the STT in the module were implemented in the simulator, as listed in Table 2.

Table 2: Available angular velocity - maximum slew rate

STT	Value
Earth rejection angle	27 deg
Sun rejection angle	45 deg
Available angular velocity	5 deg/s (assumed)
Cross-boresight uncertainty	6 arcsec
About-boresight uncertainty	40 arcsec

Actuator models

The performance of the three-axis RWs was evaluated in the simulator. The maximum number of rounds per minute (RPM) of the reaction wheel assembly was as 6000 RPM in the XACT-50 module. The details of the reaction wheel performance are presented in Table 3. The actuator was operated at a frequency of 1 Hz using an attitude control (AC) maneuver, as shown in Figure 3. The attitude determination (AD) and AC maneuvers are allocated for the former (F) and the latter (L) 0.5 s, respectively, within an interval of 1 s. The AC with the actuator is always preceded by the AD with the STT after the generation of control commands using the relative navigation technique. The AD and AC loops enable the successful integration of the orbit and attitude determination and control algorithms with the given actuator model.

Table 3: Reaction wheel performance

Three-axis RWs	Value
Maximum torque	7 mNm
Maximum RPM	6000 RPM
Maximum angular momentum	50 mNms
RPM control resolution	0.2 RPM

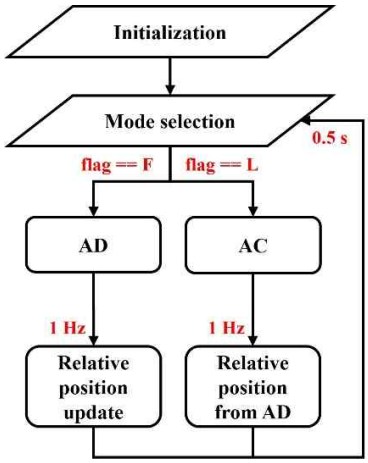

Figure 3: Integration of orbit and attitude determination & control algorithm

Navigation models

To generate attitude commands for body pointing in the ADCS module, we utilize a real-time relative navigation algorithm to align the spacecraft body and its payload with respect to the LOS vector. Owing to the long baseline formation-flying scenarios of VISION, dual-frequency (L1/L2) global positioning system (GPS) receivers are required to correct the ionospheric delay. Based on an accurate carrier-phase-based differential global positioning system (CDGPS) technique, a real-time relative navigation technique has been developed using a modified adaptive Kalman filter (MAKF) with the least-squares ambiguity decorrelation adjustment (LAMBDA) method as an integer ambiguity resolution (IAR) technique.[23] It is also essential to overcome the instability and complexity of calculations by implementing an onboard filter with single-differenced (SD) data and attaching integer ambiguity resolution process in double-differenced (DD) format. The GPS measurements were generated using a GPS signal generator (GSS 6560, Spirent) and a dual-frequency receiver (OEM719, NovAtel). However, the GNSS signal generator SimGEN can only generate a single-

frequency (L1) signal. Therefore, it is necessary to overcome the frequency-type limitation by modeling the L2 signal to correct the ionospheric delay based on the definition of the pseudorange and carrier-phase measurements using Equations (2) and (3): According to Kim et al[23], the pseudo-GNSS signals have been successfully verified and used to conduct hardware simulations for real-time relative navigation.

$$P_{L2}^{j} = P_{L1}^{j} - I_{L1}^{j} + \frac{f_{L1}^{2}}{f_{L2}^{2}} I_{L1}^{j} + \varepsilon_{P}^{j} \quad (2)$$

$$\Phi_{L2}^{j} = -\frac{\left(\mathrm{A}_{L1}^{j}\lambda_{L1} - I_{L1}^{j} + \frac{f_{L1}^{2}}{f_{L2}^{2}} I_{L1}^{j} + \varepsilon_{\Phi}^{j}\right)}{\lambda_{L2}} + N_{L2}^{j}, \quad (3)$$

where $P_{L1/L2}^{j}$ and Φ_{L2}^{j} illustrate the modeled pseudorange and carrier-phase measurement, A_{L1}^{j} is the accumulated doppler range from OEM719, I_{L1}^{j} indicates ionospheric path delay obtained from SimGEN, $\lambda_{L1/L2}$ and $f_{L1/L2}$ are the signal wavelength and frequency, N_{L2}^{j} is the ambiguities, $\varepsilon_{P/\Phi}^{j}$ is the unmodeled errors for GPS satellite j. The initial settings of the SimGEN software are described symmetrically for the two 6U nanosatellites in Table 4.

Table 4: Initial setting of the SimGEN

Property	Specification
Mass	9.3 kg
Gravity model	JGM-3 70 × 70
Solar radiation pressure	1.8
Drag coefficient	2.2
Solar radiation pressure area	0.14 m^2
Drag area	0.06 m^2
Clock model	Gauss-Markov 2nd order
TEC model	Constant TEC

Using pseudo-GNSS signals, real-time relative navigation processes and updates their positions at a frequency of 1 Hz. The mask angle was set to 5° to mitigate signal degradation at lower elevations owing to atmospheric effects. The estimated relative position is converted into a 2D plane in the radial normal (RN) direction. This can assist in generating an attitude control command to precisely align the LOS vectors of the two formation-flying satellites.

Mission scenarios

Among the five baseline scenarios (50, 100, 200, 500, and 1,000 km) in the along-track direction of the VISION mission, an integrated orbit-attitude simulator was designed for the two formation-flying CubeSats in a 1,000 km and LEO environment. The initial satellite properties specified for the moment of inertia (MOI), cross-sectional area, initial attitude, and disturbance forces are listed in Table 5. The initial attitude was selected randomly because we could not determine the exact attitude of the satellite when beginning the PAT sequence.

Table 5: Initial satellite properties

Property	Value
Moment of inertia (MOI)	$\begin{bmatrix} 13052385 & -55644.52 & 58407.480 \\ -55644.625 & 9462083.2 & -424356.93 \\ 58407.480 & -424356.93 & 5748631.7 \end{bmatrix} \times 10^{-8} kg\,m^2$
Cross section	$0.3 \times 0.2\ m^2(+X)$ $0.3 \times 0.2\ m^2(+Y)$ $0.3 \times 0.2\ m^2(-Z)$
Attitude	$(q1, q2, q3, q4)$ $= (-0.18785971463104, -0.225933744612361,$ $0.141650530338817, 0.438179527313868)$
RWs	200 RPM

The satellite orbits were sun-synchronous at an altitude of 600 km, with a local time of ascending node (LTAN) of 18h on March 22, 2026, at 16:00:00 (UTC). The two CubeSats were aligned in the along-track direction, which made a difference in the orbital elements only in the true anomaly (TA), as shown in Table 6.

Table 6: Orbital elements

Sun synchronous orbit (SSO)	Semi-major axis	6,978.137 km
	Eccentricity	5.785734×10^{-10}
	Inclination	97.93904°
	Right ascension of the ascending node	89.83343°
	Argument of periapsis	357.4668°
	True anomaly (Altair)	2.530662°
	True anomaly (Vega)	10.74865°

By applying the CubeSat bus properties, pointing bias, and loss in the combined orbit-attitude simulator, we investigated the PAT sequence to test and validate the mission operations and performance of the precise pointing techniques.

The overall orbit-attitude integrated algorithm starts with the initialization of the VISION mission scenario, as shown in Figure 4. The sequential attitude determination and control system with GPS-based relative navigation are then operated to conduct the BIS and CPS before entering the FSM feedback system because the payload is not built into the simulator. Throughout the PAT sequences of the BIS and CPS with the CAM feedback, an integrated orbit-attitude-pointing system was used to maintain the position and alignment of the CubeSat bus.

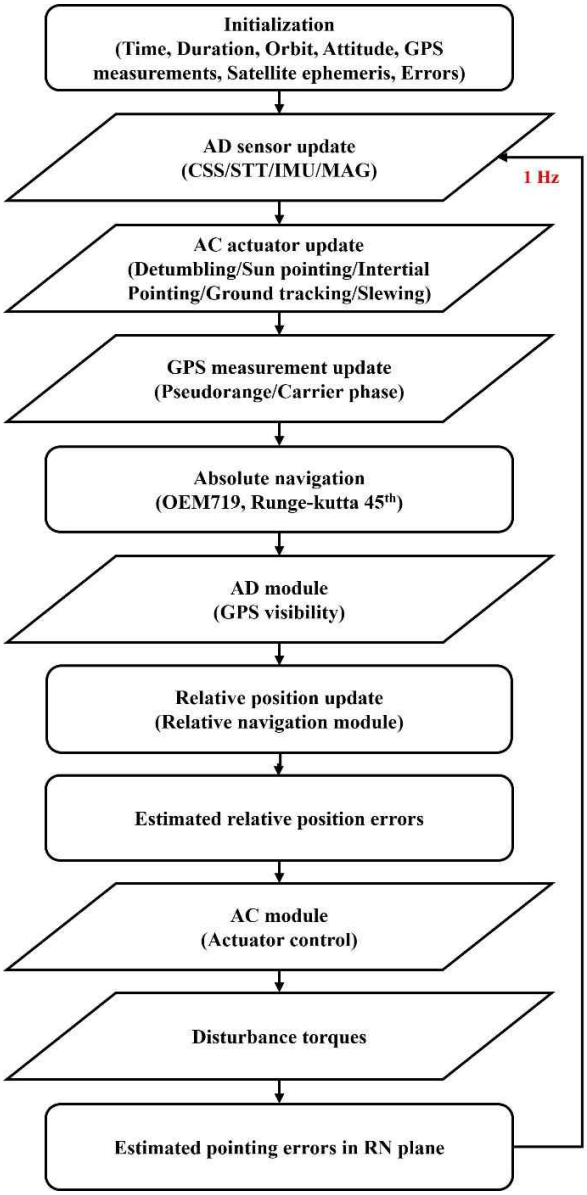

Figure 4: Flow of the integrated orbit-attitude simulator

TEST RESULTS

An integrated orbit-attitude simulator was used to analyze the pointing performance of two 6U nanosatellites in formation flight as part of the VISION mission. The worst-case scenario was set at a 1,000 km baseline for 1,500 s. The pointing accuracy during the BIS and CPS with CAM-On and the relative navigation performance were investigated considering the specifications of the integrated ADCS module in the PAT sequence.

Although unable to perfectly emulate the internal algorithm of XACT-50, the current simulator is designed to achieve attitude determination and control performance that closely resembles that of XACT-50. This implies that the specifications of the hardware components are incorporated in the AD and AC systems with the ST and RWs attributes provided by Blue Canyon Technologies. The hardware performance of the integrated ADCS was applied to model the attitude control behavior and generate attitude uncertainties using a noise filter. The initial design of the simulator was developed by Kim[24], and reasonable on-orbit conditions were replenished by adjusting the control frequency and boresight pointing architecture, implementing simultaneous relative navigation, and time synchronization.

Pointing accuracy

The initial bias of the pointing error was set to 100 arcs. The accumulated alignment errors were then estimated based on the dataset from the previous 30 s during BIS. We built a control feedback loop to compensate for biased attitude errors, accumulating 30 s of correlation with a frequency of 1 Hz. After 500 s, the CPS begins to calibrate the pointing bias with real-time LOS errors, which mainly assist in CPS acquisition. Closed-loop CAM feedback was executed to align the two satellites precisely using the AOA calibration. Figure 5 shows that the PAT sequence begins with the BIS by detecting the laser beam with an initial bias of 100 arcsec. The pointing bias is then successfully calibrated in the CPS, obtaining only 2.1 arcsec (3σ) of bias from the origin.

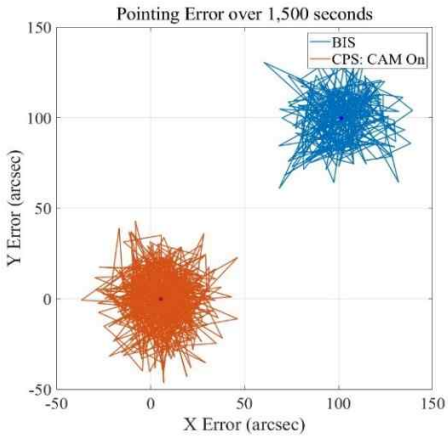

Figure 5: Pointing accuracy of the BIS and CPS

The origin indicates the full field of view (FFOV) center of the Vega with respect to Altair. From the simulation results, we conclude that the pointing performance in the CPS satisfies the total body pointing budget within 90 arcsec (3σ), yielding the total 46.9 arcsec (3σ) of

pointing uncertainty from 100 times Monte Carlo simulation.

Figures 6 and 7 show the time series of the total pointing error and the pointing performance for each axis in the RN direction. For achieving the coarse pointing, the estimated LOS error must be reduced less than 1745 μrad in the FFOV of the CAM for a broad beam transmission and the beam detection. At 500 s, the CAM feedback was successfully initiated, and the pointing bias of 100 arcsec was reduced by the attitude maneuvers. The CPS search was conducted immediately when the CAM was turned on at 500 s with a duration of 60 s, and then the CPS acquisition was promptly activated to calibrate and reduce the pointing bias. CPS acquisition must be performed within 180 s to move onto CPS detection in an on-orbit scenario. In this study, we tested the acquisition procedure for 1,000 s for a more detailed investigation of the CPS. The total pointing error was calculated as the root mean square (RMS) errors in the radial and normal directions. Both the total pointing error and the uncertainties in the RN axis satisfy the mission requirements, which guarantee the alignment of the LOS vectors to establish and maintain stable intersatellite laser crosslinks.

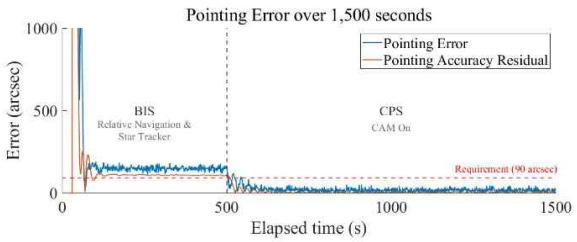

Figure 6: Timeseries of total pointing error

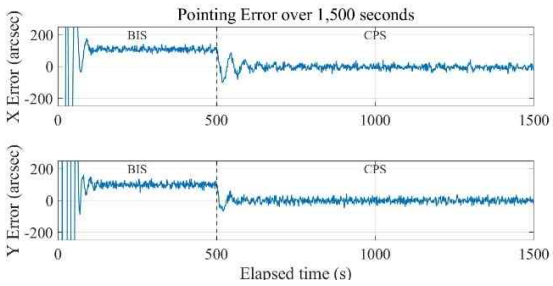

Figure 7: Timeseries of pointing error in each axis

A Rician distribution was applied to handle the estimated errors to investigate the effects of pointing errors in laser communication effectively, as demonstrated by Grenfell et al[26]. Using the confirmed statistical model, the pointing error after CPS acquisition was analyzed, as shown in Figure 8. This confirms the total pointing error of 47.9 arcsec (3σ) by modeling the Rician distribution with a 99.7% confidence limit.

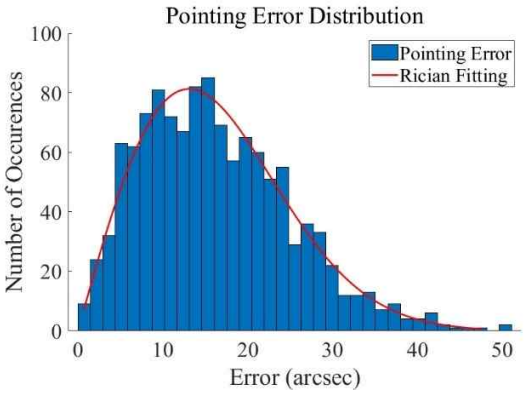

Figure 8: Rician distribution of total pointing error

Positioning accuracy

Whereas the performance of the primary pointing system is investigated within the RN plane, which heads toward the mutual LOS vectors of the payloads, the positioning performance is tested based on the LOS vectors of the geometric center in the CubeSat body. A real-time relative navigation technique is required to determine attitude control commands in the ADCS module. The positioning accuracy in the VISION mission was less than 1 m for each axis in an Earth-centeredEarth-fixed (ECEF) coordinate system. The positioning errors were investigated to analyze the 3D position estimation performance of the relative navigation system. Figures 9 and 10 show the 3D positioning uncertainties, which were relatively larger in the BIS than in the CPS, as the initial GPS ambiguities require time to converge. During the CPS, we can observe that the relative navigation accuracy is maintained less than 1 m for each axis: 0.781 m (3σ) in 3D and 0.704 m (3σ), 0.524 m (3σ), 0.251 m (3σ), respectively, in radial, tangential and normal directions by Rician distribution with 99.7% confidence.

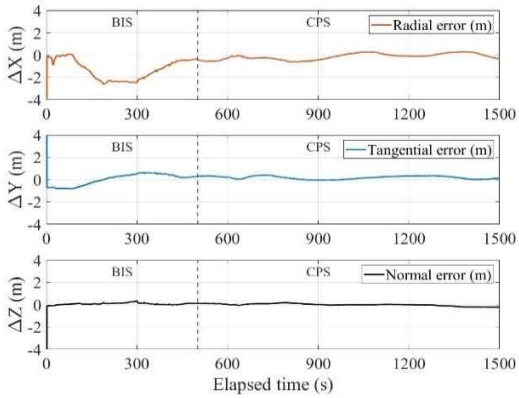

Figure 9: Timeseries of positioning error in each axis

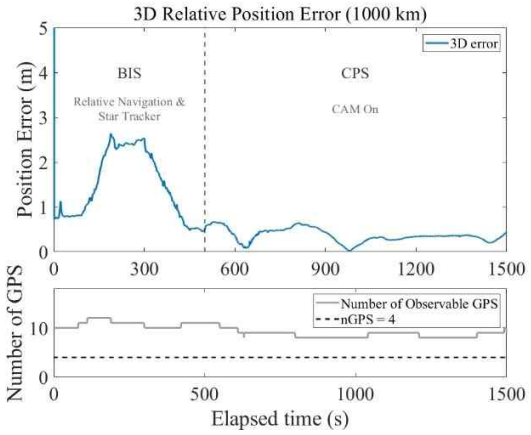

Figure 10: Timeseries of total positioning error with the number of GPS satellites

CONCLUSIONS

To test and validate the PAT sequence of the BIS and CPS with CAM feedback, an orbit-attitude integrated simulator was developed as part of the VISION mission. Owing to the restricted SWaP constraints of CubeSat platforms, the coarse pointing system primarily relies on CAM feedback and an integrated ADCS module to lower the complexity of the overall pointing system. Based on GPS-based relative navigation, the BIS initially calculates the LOS vectors of the two formation-flying satellites, and control commands are generated for the ADCS module with the star tracker. The mission scenario was implemented by applying the characteristics of the CubeSat, absolute and relative navigation systems, star trackers, and control hardware in the XACT-50 module. The orbit-attitude integrated simulator and its numerical assessment results demonstrated that the proposed design of the 6U CubeSat yields the total body pointing error of 46.9 arcsec (3σ) during the PAT sequence, indicating that the attitude control system combined with the developed navigation model satisfies the mission requirements on the PAT system. Therefore, two formation-flying CubeSats can achieve a super-high data-transmission rate of 1 Gbps, to be maintained for over 10 min. In conclusion, this study provides the details of developing an orbit-attitude integrated simulator and analyzes the performance of the PAT system in the VISION mission scenario, mainly focusing on the BIS and CPS with the process of CAM feedback. Future work will also include the analysis of FPS with the FSM feedback, investigating the FSM feedback loop with the LCT.

Acknowledgments

This research was supported by the Challengeable Future Defense Technology Research and Development Program through the Agency for Defense Development (ADD) and funded by the Defense Acquisition Program Administration (DAPA) in 2023 (No.915027201). This study was supported by Hyundai Motors Chung Mong-Koo Foundation.

References

1. Alliance, N. G. M. N., “Non-Terrestrial Networks Position Paper,” project: Extreme Long-Range Communications for Deep Rural Coverage, vol. 11, 2019.
2. 3GPP., “Study on New Radio (NR) to support non-terrestrial networks,” TR 38.811 V15. 2.0., 2019.
3. Twiggs, R. J, “A new generation of picosatellite for education and industry low-cost space experimentation,” In AIAA/USU Small Satellite Conference Proceedings V-5, 2000.
4. Chin, A., Coelho, R., Brooks, L., Nugent, R. and Puig-Suari, J., “Standardization promotes flexibility: a review of CubeSats’ success,” Aerospace Engineering, vol. 805, pp. 756-5087, 2008.
5. Saeed, N., Elzanaty, A., Almorad, H., Dahrouj, H., Al-Naffouri, T. Y. and Alouini, M. S., “CubeSat communications: Recent advances and future challenges,” IEEE Communications Surveys & Tutorials, vol. 22, No. 3, pp.1839-1862., 2020.
6. Scholz, A., Giesselmann, J. and Duda, C., “CubeSat technical aspects,” In 55th International Astronautical Congress of the International Astronautical Federation, the International Academy of Astronautics, and the International Institute of Space Law, pp. P-5, 2004.
7. Tummala, A. R. and Dutta, A., “An overview of cube-satellite propulsion technologies and trends,” Aerospace, vol. 4, No. 4, pp. 58, 2017.
8. Welle, R. P., Janson, S., Rowen, D. and Rose, T., “CubeSat-scale laser communications,” In 31st Space Symp, April 2015.
9. Kaushal, H. and Kaddoum, G., “Optical communication in space: Challenges and mitigation techniques,” IEEE communications surveys & tutorials, vol. 19, No. 1, pp. 57-96, 2016.
10. Carrasco-Casado, A., Biswas, A., Fields, R., Grefenstette, B., Harrison, F., Sburlan, S. and Toyoshima, M., “Optical communication on CubeSats—Enabling the next era in space science,” In 2017 IEEE International Conference on Space Optical Systems and Applications (ICSOS), IEEE, pp. 46-52, November 2017.

11. Kingsbury, R. W., Nguyen, T., Riesing, K. and Cahoy, K., “Fast-steering solutions for cubesat-scale optical communications,” In International Conference on Space Optics—ICSO 2014, SPIE, vol. 10563, pp. 124-130, November 2017.

12. Rose, T. S., Rowen, D. W., LaLumondiere, S., Werner, N. I., Linares, R., Faler, A., Wicker, J., Coffman, C. M., Maul, G. A., Chien, D. H., Utter, A., Welle, R. P. and Janson, S. W., “Optical communications downlink from a 1.5 U CubeSat: OCSD program,” In International Conference on Space Optics—ICSO 2018, SPIE, vol. 11180, pp. 201-212, July 2019.

13. Sansone, F., Francesconi, A., Corvaja, R., Vallone, G., Antonello, R., Branz, F. and Villoresi, P., “LaserCube optical communication terminal for nano and micro satellites,” Acta astronautica, vol. 173, pp. 310-319, 2020.

14. Pimentel, P. M., Rödiger, B., Schmidt, C., Fuchs, C., Rochow, C., Hiemstra, T., Zager, A., Wertz, P., Knopp, M., Lehmann, M. and Mrowka, F., “Cube laser communication terminal (CubeLCT) state of the art,” Acta Astronautica, vol. 211, pp. 326-332, 2023.

15. Chaudhry, A. U. and Yanikomeroglu, H., “Laser intersatellite links in a starlink constellation: A classification and analysis,” IEEE Vehicular Technology Magazine, vol. 16, No. 2, pp. 48-56, 2021.

16. Rödiger, B., Menninger, C., Fuchs, C., Grillmayer, L., Arnold, S., Rochow, C., Wertz, P. and Schmidt, C., “High data-rate optical communication payload for CubeSats,” In Laser Communication and Propagation through the Atmosphere and Oceans IX, SPIE, vol. 11506, pp. 12-24, August 2020.

17. Schmidt, C., Rödiger, B., Rosano, J., Papadopoulos, C., Hahn, M. T., Moll, F. and Fuchs, C., “DLR's Optical Communication Terminals for CubeSats,” In 2022 IEEE International Conference on Space Optical Systems and Applications (ICSOS), IEEE, pp. 175-180, March 2022.

18. Kammerer, W., Grenfell, P., Hyest, L., Serra, P., Tomio, H., Belsten, N., Lindsay, C., Cierny, O., Cahoy, K., Clark, M., Coogan, D., Conklin, J., Mayer, D., Stupl, J. and Hanson, J., “CLICK mission flight terminal optomechanical integration and testing,” In International Conference on Space Optics—ICSO 2022, SPIE, vol. 12777, pp. 1292-1307, July 2023.

19. Cahoy, K., Grenfell, P., Crews, A., Long, M., Serra, P., Nguyen, A., Fitzgerald, R., Haughwout, C., Diez, R., Aguilar, A., Conklin, J., Payne, C., Kusters, J., Sackier, C., LaRocca, M. and Yenchesky, L., “The CubeSat laser infrared crosslinK mission (CLICK),” In International Conference on Space Optics—ICSO 2018, SPIE, vol. 11180, pp. 358-369, July 2019.

20. Kim, G.-N., Park, S.-Y., Seong, S., Lee, J., Choi, S., Kim, Y.-E., Ryu, H.-G., Lee, S., Choi, J.-Y. and Han, S.-K., “The Vision – concept of laser crosslink systems using nanosatellites in formation flying,” Acta Astronautica, vol. 211, pp. 877–897. October 2023.

21. Kim, G. N., Park, S. Y., Seong, S., Choi, J. Y., Han, S. K., Kim, Y. E., Choi, S., Lee, J., Lee, S., Ryu, H. G. and Kim, S., “Design of Novel Laser Crosslink Systems Using Nanosatellites in Formation Flying: The VISION,” Aerospace, vol. 9, No. 8, pp. 423, 2022.

22. Odijk, D., “Ionosphere-free phase combinations for modernized GPS,” Journal of surveying engineering, vol. 129, No. 4, pp. 165-173, 2003.

23. Kim, Y., Kim, P., Ryu, H. G. and Park, S. Y., “Evaluating the On-Orbit Relative Navigation Performance of Modified Adaptive Kalman Filter with GPS Ambiguity Resolution,” In Proceedings of the 2024 International Technical Meeting of The Institute of Navigation, pp. 658-676, January 2024.

24. Kim, Y. E., “Attitude controller design and analysis of micro-satellite for free space optical communication (FSOC),” Master's thesis, Yonsei University, 2023.

25. Chang, J., Schieler, C. M., Riesing, K. M., Burnside, J. W., Aquino, K. and Robinson, B. S., “Body pointing, acquisition and tracking for small satellite laser communication,” In Free-Space Laser Communications XXXI, SPIE, vol. 10910, pp. 144-152, March 2019.

26. Grenfell, P., Aguilar, A., Cahoy, K. and Long, M., “Pointing, acquisition, and tracking for small satellite laser communications,” In AIAA/USU Small Satellite Conference Proceedings, 2018.